DALTON
FULL PAPER

Magnetic properties of a bishelical [4 + 4 + 4] trinuclear copper(II) complex

Jesús Sanmartín,[a] Manuel R. Bermejo,*[a] Ana M. García-Deibe,[a] Otaciro R. Nascimento,[b] Luis Lezama[c] and Teófilo Rojo[c]

[a] *Dpto. de Química Inorgánica, Facultade de Química, Universidade de Santiago de Compostela, E-15706 Santiago de Compostela, Galicia, Spain. E-mail: qisuso@usc.es*
[b] *Instituto de Física de São Carlos, Universidade de São Paulo, C.P. 369, 13560-970 São Carlos, SP, Brazil*
[c] *Dpto. de Química Inorgánica, Facultad de Ciencias, Universidad del País Vasco. B° Sarriena s/n, 48940 Leioa, Bilbao, Spain*

Received 1st August 2001, Accepted 11th December 2001
First published as an Advance Article on the web 12th February 2002

A peculiar [4 + 4 + 4] trinuclear Cu(II) bishelicate has been studied by X-ray diffraction techniques, FT–IR and UV–Vis spectroscopies, magnetic measurements and EPR spectroscopy. Magnetic susceptibility studies indicate a strong antiferromagnetic interaction ($J/k = -194$ K) between the three copper ions in the bishelicate. The existence of antiferromagnetic intermolecular interactions ($z'J'/k = -0.91$ K) was also determined. In spite of the presence of two magnetically different centres, only one signal is observed due to the exchange effects. Below 100 K the linewidth of the signals rapidly decreases and a typical exchange narrowed spectrum is observed at 4 K. The main contribution to the ground state wave function can be attributed to the $d_{x^2-y^2}$ orbitals, as expected for tetrahedrally distorted planar square Cu(II) chromophores.

Introduction

The investigation on physical and physicochemical properties of complexes containing two or more metal centres in close proximity is a very important research area, which has led to the proposal of several models for some biochemical processes.[1–7] These have contributed to a better knowledge of oxygen transport and activation by metalloenzymes, as well as of some industrial catalytic processes.[8]

Ascorbate oxidase and laccase are copper enzymes[9] that catalyze oxidation of a substrate with the concomitant $4e^-$ oxygen reduction. They contain four copper atoms per functional unit, one of them (bound in a mononuclear complex) is involved in the electron uptake from the substrate. The remaining three Cu(II) binding sites are arranged as an isosceles triangle with Cu ··· Cu distances in the range 3.66–3.90 Å and constitute a trinuclear complex, which is the catalytic oxygen reduction site.[9] This complex, in the oxidized state, consists of a pair of antiferromagnetically coupled Cu(II) ions (with a bridging O-donor ligand),which are EPR silent, and a Cu(II) ion, EPR active. Spectroscopic and chemical studies of laccase and ascorbate oxidase trinuclear copper active sites have been reported.[10] Some efforts to synthesize trinuclear copper complexes comprising this type of metal arrangement[11,12] have been recently communicated. The relationship between the peculiar spectroscopic properties of polynuclear complexes and their structural features is crucial to characterize protein models and can help in the understanding of reaction mechanisms or reaction details at the active site.

We have previously communicated the direct electrochemical synthesis and the X-ray crystal structure at 293 K of an exciting trinuclear bishelicate with an isosceles triangle core self-assembled by two μ-phenoxo bridges [Cu ··· Cu: 3.413(3) and 3.858(3) Å].[12] The tetracoordinated Cu ions are in tetrahedrally distorted square planar environments. Two of the copper ions are in NO_3 environments and the remaining one forms a CuN_2O_2 chromophore.

Here, we describe the study by X-ray diffraction techniques, FT–IR and UV–Vis spectroscopies, magnetic measurements and EPR spectroscopy of $Cu_3(H_2L)(L)\cdot 2H_2O$ [H_4L = *N*,*N*′-bis(3-hydroxysalicylidene)-1,4-diaminobutane (Scheme 1)] as a function of temperature, which acts as a modulator of some slight structural changes.

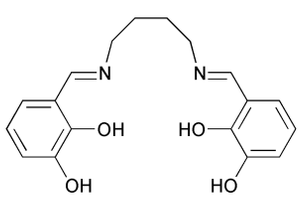

Scheme 1 Schematic representation of H_4L.

Results and discussion

A brief account of the $[Cu_3(H_2L)(L)]\cdot 2H_2O$ crystal structure at 293 K has been previously published.[12] Preliminary magnetic studies of a powder sample seemed to indicate that the temperature could influence the structure. Since the tetramethylene spacer was disordered and some crystal parameters were not optimum, new single crystal X-ray diffraction measurements have been performed at 100 K. Our aim was to improve the crystal data and to establish or discard a possible phase transition. Likewise, they were repeated at 293 K, in order to compare all the structural parameters with strict scientific rigour. Thus, we can tell now that only subtle structural changes could be detected, but the quality of data and *R* indices have been significantly improved. These structural changes will be discussed, as well as some other aspects not previously commented upon.

X-Ray single crystal diffraction studies at 100 K of $[Cu_3(H_2L)(L)]\cdot 2H_2O$

Fig. 1 shows the [4 + 4 + 4] bishelicate lying upon a two-fold

 DOI: 10.1039/b106983g

Table 1 Most significant bond lengths (Å) and angles (°) for $Cu_3(H_2L)(L)\cdot 2H_2O$

Bond/Å	100 K	293 K
Cu(1)–O(10)	1.8989(16)	1.8959(18)
Cu(1)–O(21)	1.9195(16)	1.9200(19)
Cu(1)–N(16)	1.952(2)	1.955(2)
Cu(1)–O(20)	1.9653(16)	1.9639(19)
Cu(2)–O(20)	1.9119(17)	1.9130(19)
Cu(2)–O(20A)	1.9119(17)	1.9130(19)
Cu(2)–N(26)	1.933(2)	1.935(2)
Cu(2)–N(26A)	1.933(2)	1.935(2)
O(10)–C(10)	1.319(3)	1.318(3)
O(11)–C(11)	1.365(3)	1.358(4)
O(20)–C(20)	1.341(3)	1.348(3)
O(21)–C(21)	1.348(3)	1.343(4)
N(16)–C(16)	1.290(3)	1.285(4)
N(26)–C(26)	1.281(3)	1.280(4)
Interatomic distances/Å		
Cu(1) ··· Cu(1A)	3.8385(9)	3.8640(10)
Cu(1) ··· Cu(2)	3.4241(16)	3.4259(7)
N(16) ··· N(16A)	4.500(4)	4.516(5)
N(26) ··· N(26A)	3.011(4)	3.012(5)
O(10) ··· O(10A)	5.081(3)	5.123(4)
O(11) ··· O(11A)	8.508(4)	8.532(5)
O(20) ··· O(20A)	2.808(3)	2.823(4)
O(21) ··· O(21A)	5.782(3)	5.801(4)

Angle/°	100 K	293 K
O(10)–Cu(1)–N(16)	95.12(7)	95.01(9)
O(21)–Cu(1)–N(16)	97.55(8)	97.77(10)
O(10)–Cu(1)–O(20)	88.65(7)	88.79(8)
O(21)–Cu(1)–O(20)	84.25(7)	84.20(8)
N(16)–Cu(1)–O(20)	158.98(8)	158.81(10)
O(20)–Cu(2)–O(20A)	94.50(10)	95.10(12)
O(20)–Cu(2)–N(26)	95.75(8)	95.68(10)
O(20A)–Cu(2)–N(26)	138.69(8)	138.50(9)
O(20A)–Cu(2)–N(26A)	95.75(8)	95.68(10)
N(26)–Cu(2)–N(26A)	102.32(12)	102.18(15)
Cu(2)–O(20)–Cu(1)	124.04(8)	124.17(9)
C(10)–O(10)–Cu(1)	126.73(15)	126.84(18)
C(16)–N(16)–Cu(1)	122.88(16)	122.5(2)
C(17)–N(16)–Cu(1)	120.06(15)	119.78(19)
C(20)–O(20)–Cu(1)	111.33(15)	111.28(18)
C(21)–O(21)–Cu(1)	111.36(15)	111.29(18)
C(20)–O(20)–Cu(2)	124.23(15)	124.11(18)
C(26)–N(26)–Cu(2)	122.47(17)	122.4(2)
C(27)–N(26)–Cu(2)	119.7(2)	112.4(9)
C(27′)–N(26)–Cu(2)		130.0(11)
Torsion angles/°		
N(16)–C(17)–C(18)–C(18A)	58.8(3)	59.0(2)
N(26)–C(27)–C(28)–C(28′A)	44.2(17)	29.0(6)
C(27)–C(28)–C(28′A)–C(27′A)	62.8(19)	
C(27)–C(28)–C(28′A)–C(27A)		65.2(7)
N(26)–C(27′)–C(28′)–C(28A)	−81(2)	

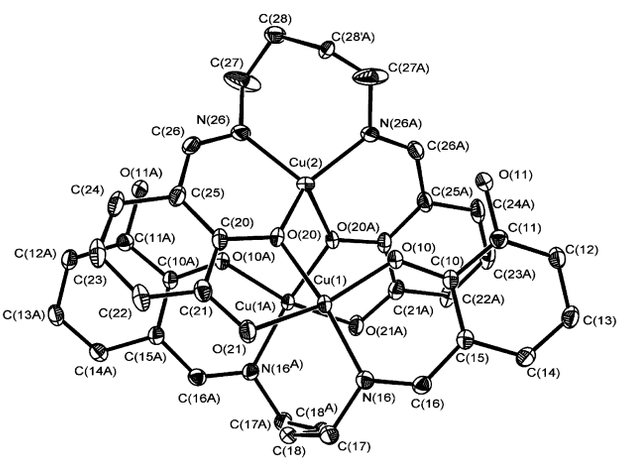

Fig. 1 ORTEP representation (50% probability) of $Cu_3(H_2L)(L)\cdot 2H_2O$ at 100 K.

axis on Cu(2). Two μ-phenoxo bridges assemble its isosceles triangular core, where the Cu(II) environments could be described as tetrahedrally distorted square planar. This type of trinuclear array is reminiscent of that found for some copper enzymes as the oxidized ascorbate oxidase,[9] where the shortest Cu ··· Cu distance (3.66 Å) also presents an O-bridge. In our case, two of the Cu(II) ions are crystallographically equivalent, since half molecule is generated by the symmetry operation $-x$, y, $0.5 - z$, these atoms being denoted by 'A'. These two ions are placed on the triangle base, with the longest Cu ··· Cu distance (3.86 Å) being connected by the $(CH_2)_4$ spacer. Some selected distances and angles are listed in Table 1.

The severely distorted geometry around Cu(2) comprises the N_2O_2 inner compartment of L^{4-}. The half-stepped distances of the donor atoms to the least-squares calculated N_2O_2 plane (*ca.* ±0.63 and ±0.71 Å) and the angle formed by the two chelate planes (53°) show this distortion. This geometry suffers a slight variation at 100 K, which could be considered as mostly related to the *ca.* 0.6° closing of the O(20)–Cu(2)–O(20A) angle. The other two copper centres are in more square planar NO_3 chromophores achieved through O(20), which forms a μ-phenoxo bridge to Cu(2), and O(21) corresponding to L^{4-}, while O(10) and N(16), belonging to H_2L^{2-}, complete the coordination sphere.

Distances and angles involved in the metal environments do not show significant differences at both temperatures, as Table 1 shows, but the combination of slight changes lead to a lower planarity of Cu(1) at 100 K. This is deduced from the slight decrease (*ca.* −0.006 Å) found for N(16), O(10), O(21) and O(20) of the half-stepped distances to the least-squares calculated chromophore plane. Curiously, the angle formed by both chelate planes [N(16)–C(16)–C(15)–C(10)–O(10) and O(20)–C(20)–C(21)–O(21)] decreases from 26.83(9)° at 293 K to 26.32(8)° at 100 K.

It could be noteworthy, especially for IR studies, that when the ligand is tetra-deprotonated and fully coordinated, as L^{4-}, both C–O bonds show a nearly single bond character (Table 1), and they seem inversely affected by the temperature change. However, in the case of H_2L^{2-}, coordinated O(10) shows a marked double bond character, whereas the protonated O(11) is clearly single-bonded to C(11), and is even elongated at low temperature.

The most relevant changes observed after decreasing temperature at 100 K correspond to the $(CH_2)_4$ chain of L^{4-} (Fig. 2). This spacer shows a pronounced twisted, as torsion angles of

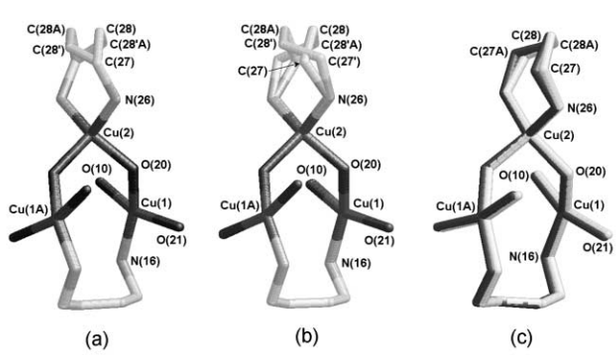

Fig. 2 Partial view of $Cu_3(H_2L)(L)\cdot 2H_2O$ excluding aromatic rings, iminic C-atoms and uncoordinated O-atoms, and showing the disordered spacers at (a) 100 K and (b) 293 K. (c) A superimposition of (a) pale and (b) dark, showing the subtle differences at both temperatures, only considering the C(27) and C(28) positions.

both chains confirm (Table 1), so that the atom positions seem to be forced and cause their disorder. This uncertainty appears even at low temperature, but with less incidence, since C(27) occupies only one position, whereas it can occupy two different ones at 293 K. The central atoms of this chain remain disordered in any case, showing *ca.* 50% occupation sites for C(28) and C(28′). These changes do not seem to influence on the intramolecular distances between equivalent donor atoms. Curiously, the ones most affected are those corresponding to H_2L^{2-}, which are slightly elongated at 100 K (Table 1). It could be remarkable that C(28) is bonded to C(28′A), and inversely C(28′) to C(28A). This leads to a crystallographic equivalence between both disordered chains, by a mere 180° turn ($-x$, y, $0.5 - z$).

Despite the L^{4-} coiling and the steric hindrance between both ligand units, stacking interactions between the aromatic rings of both helical threads appear to exist. The 3-hydroxysalyicylidene residues display a rather high planarity in all the cases. Thus, the highest value found for angles formed between chelate planes and their related aromatic rings is 4.01(5)°, which corresponds to C(10)–C(11)–C(12)–C(13)–C(14)–C(15) and N(16)–C(16)–C(15)–C(10)–O(10), at 100 K.

Vibration spectra

Room temperature Raman spectroscopic studies of $Cu_3(H_2L)(L)\cdot 2H_2O$ were unsuccessful, since radiation causes its decomposition. The most characteristic mid-infrared bands have been assigned following the literature.[13–15] The sharp band due to the phenol OH groups (3222 cm^{-1} for H_4L) disappears in the complex spectrum, and a very broad band at 3431 cm^{-1}, attributable to solvated water molecules, is now present. The observation of a sharp band related to the remaining hydroxy groups could be expected, but the water OH band obscures it.

At room temperature, the ν(C=N) and ν(C–O) modes are present for $Cu_3(H_2L)(L)\cdot 2H_2O$ as two very strong bands at 1623 and 1268 cm^{-1}, respectively. The significant shift evidenced by these signals (-7 and $+31$ cm^{-1}) in the complex spectrum indicates that the ligand is coordinated *via* N and O atoms. Consecutive falls in temperature to 224, 110 and 82 K do not seem to prompt a change in the ν(C=N) and ν(C–O) band positions (1623 and 1267 cm^{-1}, respectively). However, the strong band centred at 1458 cm^{-1} is split in two bands, at 1458 and 1464 cm^{-1}, at low temperatures.

The observation at 293 K of two weak bands at 1556 and 1592 cm^{-1} (1546 cm^{-1} in H_4L) allows us to postulate some degree of multiple bond[13] attributable to $\nu(C{=}O)_{phenolate}$, as the crystal structure confirms. When the spectrum is taken below 224 K, these bands appear unaffected (1557 and 1594 cm^{-1}).

Ligand coordination to the copper centre is substantiated by two bands, at 465 (medium) and 320 (strong) cm^{-1}, attributable to ν(Cu–N) and ν(Cu–O), respectively.[16] The low frequency Cu–N vibration was studied at variable temperature. From this, we can say that the Cu–N stretching vibration appears unaffected by a temperature decrease (466 cm^{-1} below 224 K).

Electronic spectra

$Cu_3(H_2L)(L)\cdot 2H_2O$ displays two medium (340 and 420 nm), one strong (300 nm), and two very strong ligand absorption bands at about 225 and 265 nm. These are clearly charge transfer transitions in origin, and this makes it difficult to observe the d–d transitions. Therefore, the electronic spectrum of $Cu_3(H_2L)(L)\cdot 2H_2O$, both in the solid state and in solution, is characterized by low-intensity absorption bands or shoulders that can be associated with d–d transitions. The electronic spectra both in ethanol and dimethyl sulfoxide solution, are rather similar and show a weak band around 670 nm and a clear shoulder at about 570 nm. This could be caused by the two different copper environments found: quasi square planar and very tetrahedrally distorted square planar.[13,17,18]

Magnetic properties

Thermal evolution of the magnetic molar susceptibility is shown in Fig. 3 in the form of the $\chi_m T$ ($\chi_m T = \mu_{eff}^2/8$) and $1/\chi_m$

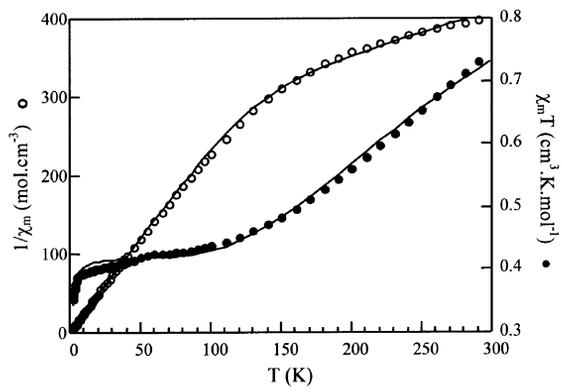

Fig. 3 Thermal evolution of $\chi_m T$ (●) and $1/\chi_m$ (○). Continuous lines correspond to the best least-squares fit.

versus T plots. The effective magnetic moment decreases from 2.45 BM at 300 K to 1.65 BM at 2 K. The room temperature $\chi_m T$ value (0.749 cm^3 K mol^{-1}) is substantially lower than that expected for three uncoupled Cu(II) ions (1.125 cm^3 K mol^{-1}, considering $g = 2$). This fact indicates the predominance of antiferromagnetic interactions in the trinuclear compound, as the rapid decrease of the effective magnetic moment with decreasing temperature confirms. Moreover, the exchange coupling must certainly be strong, considering that Curie–Weiss behaviour is not observed even at high temperatures on the reciprocal susceptibility curve.

Below 100 K the decrease observed on the $\chi_m T$ values is less pronounced, tending to the expected plateau, characteristic of an $S = 1/2$ system resulting from an antiferromagnetically coupled trinuclear Cu(II) compound. Below 10 K the effective magnetic moment shows a new rapid decrease, which can only be attributable to antiferromagnetic intermolecular interactions.

The magnetization *versus* applied field curve registered at 2 K (Fig. 4) shows saturation for an $M/N\beta$ value close to 1. This

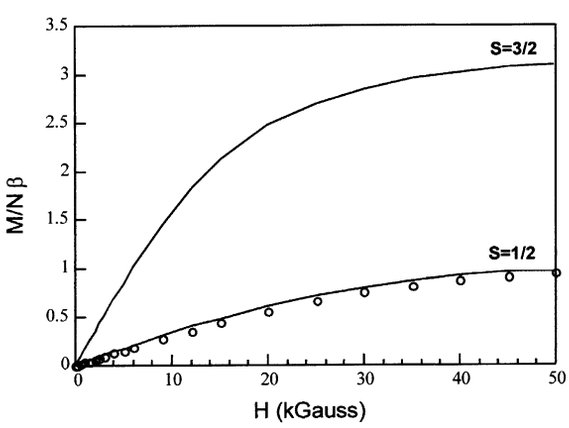

Fig. 4 Magnetization *versus* applied field plot. The solid lines correspond to the Brillouin functions for $S = 1/2$ and $S = 3/2$.

is characteristic of a trinuclear system with $S = 1/2$ and significant antiferromagnetic interactions. The experimental data are slightly lower than those calculated from the Brillouin function for $S = 1/2$. This fact also supports the existence of antiferromagnetic intermolecular interactions.

Bearing in mind the structure of this compound, we have used the following Heisenberg Hamiltonian to describe the low-lying electronic states:

$$H = -2J(S_1 \cdot S_2 + S_2 \cdot S_3 + \alpha S_1 \cdot S_3) \qquad (1)$$

Table 2 Energies of the spin states for a triangular arrangement of Cu(II) ions

S^*	S'	$-W(S')$
0	1/2	$3/2aJ$
1	1/2	$2J - 1/2aJ$
1	3/2	$-J - 1/2aJ$

Using Kambe's method,[19] the eigenvalues are given by:

$$W(S') = -J[S'(S' + 1) - (1 - a)S^*(S^* + 1) - (1 + 2a)S(S + 1)] \quad (2)$$

where S^* ($S^* = S_1 + S_3$) is the spin quantum number associated with crystallographically equivalent copper ions, Cu(1) and Cu(1A), and S' ($S' = S^* + S_2$) is the total spin of the compound. The possible values for S^* and S' together with the energy of each spin state are given in Table 2.

Application of the van Vleck's susceptibility equation and adding the Zeeman term to the precedent Hamiltonian (considering equal and isotropic g values for the three copper ions) gives the following expression for the molar susceptibility:

$$\chi_m = \frac{Ng^2\beta^2}{4kT} \frac{10\exp\left(\frac{J + 2\alpha J}{kT}\right) + \exp\left(\frac{-2J + 2\alpha J}{kT}\right) + 1}{2\exp\left(\frac{J + 2\alpha J}{kT}\right) + \exp\left(\frac{-2J + 2\alpha J}{kT}\right) + 1} \quad (3)$$

The effect of the intermolecular interactions was included by means of a J' exchange parameter treated in the Molecular Field Approximation:[20]

$$\chi_{m'} = \frac{\chi_m}{1 - \frac{2z'J'\chi_m}{Ng^2\beta^2}} \quad (4)$$

Attempts to fit the experimental curves to the above equation gave multiple solutions due to the excessive number of adjustable parameters and their strong interdependence. However, we can use a simplification of this expression if we consider $\alpha = 0$ because the exchange coupling between Cu(1) and Cu(1A) must be low due to the long exchange pathway between them (12.916 Å). The best least-squares fit (solid lines in Fig. 3) was obtained for the following values: $J/k = -194$ K, $z'J'/k = -0.91$ K and $g = 2.12$. The agreement factor $SE = [F/(n - K)]^{1/2}$ is equal to 7.4×10^{-3}, where n = no. of points (74), K = no. of adjustable parameters (3) and F = square of the residuals sum. In view of the obtained J value, the $S' = 3/2$ state population at room temperatures is obviously much lower than those corresponding to the $S' = 1/2$ states. This population decreases rapidly with temperature as the effective magnetic moment thermal evolution confirms. Below 100 K, only $S' = 1/2$ states are populated.

EPR spectroscopy

The temperature dependence of powder EPR spectra for $Cu_3(H_2L)(L)\cdot 2H_2O$ is illustrated in Fig. 5. In this figure, only representative temperatures are shown to make easier their comparison. As expected, the high temperature spectra are more complex than those observed at low temperatures. This fact is due to the contribution of signals from the $S' = 3/2$ state, together with those originated by $S' = 1/2$ states. Below 100 K the signal linewidth rapidly decreases, and a typical exchange narrowed spectrum is observed at 4 K. In spite of the presence of two magnetically different types of metal centre, only one signal is observed due to exchange effects.

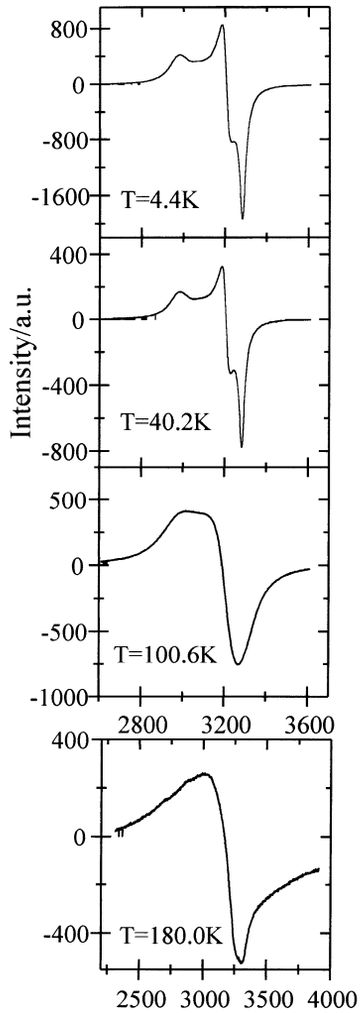

Fig. 5 X-Band powder spectra for $Cu_3(H_2L)(L)\cdot 2H_2O$ with temperature variation from 4.4 to 180 K.

In order to confirm the interpretation of powder EPR results, single crystal EPR spectra were also performed at different temperatures. Fig. 6 shows several EPR spectra in the range 10–200 K, where an exchange narrowing effect is clearly detected. It can be observed that the linewidth rapidly increases above 50 K and the signal practically disappears above 160 K. Furthermore, new contributions are also observed at high temperatures which probably are originated by the increasing population on the $S' = 3/2$ state.

The angular variation of the EPR spectra at 80 K was performed in three orthogonal planes (Fig. 7). The principal g values ($g_1 = 2.237$, $g_2 = 2.074$ and $g_3 = 2.026$) were obtained by diagonalization of the g tensor. The relationship between the crystal directions a^*, b and c (a^* is perpendicular to b and c axes) and the principal g values was found. The direction of the g_1-tensor is almost parallel to the crystal c axis (about 15° deviated) which is in accordance with the location of Cu(1) and Cu(1A). These atoms are in two coordination planes made up of Cu(1)–O(10)–O(21)–N(16) and Cu(1A)–O(10A)–O(21A)–N(16A) almost orthogonal to the c axis. The directions of the g_2- and g_3-tensors are almost parallel to b and a^* axes, respectively. Both, g_2- and g_3-tensors represent an average of the directions between Cu(1) and Cu(1A) in the cited coordination planes.

The g values obviously correspond to the resulting exchange tensor due to the exchange narrowing effect. In any case, the obtained results indicate that the main contribution to the ground state wave function can be attributed to the $d_{x^2-y^2}$ orbitals, as expected for tetrahedrally distorted square planar Cu(II) chromophores.

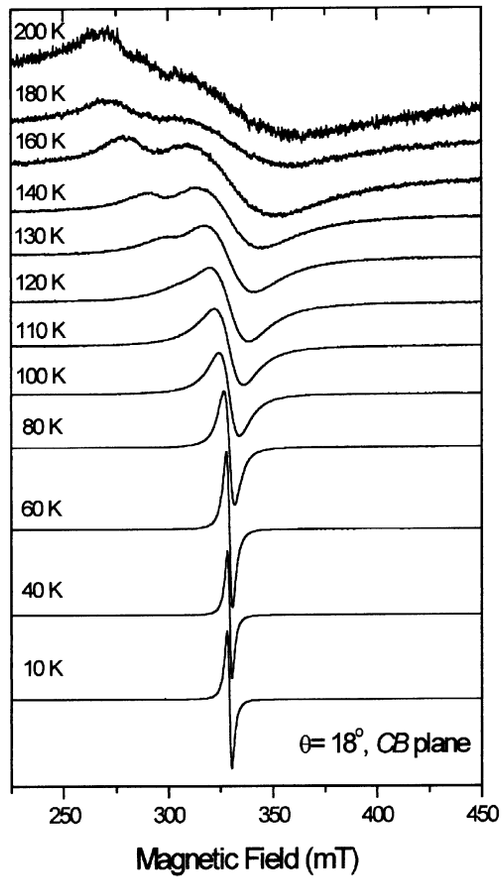

Fig. 6 Temperature variation of the single crystal EPR spectra for $Cu_3(H_2L)(L)\cdot 2H_2O$ in the direction of the *CB* plane. Microwave frequency 9484.0 MHz, microwave power 10 mW, frequency modulation 100 kHz, variable amplitude modulation and amplifier gain.

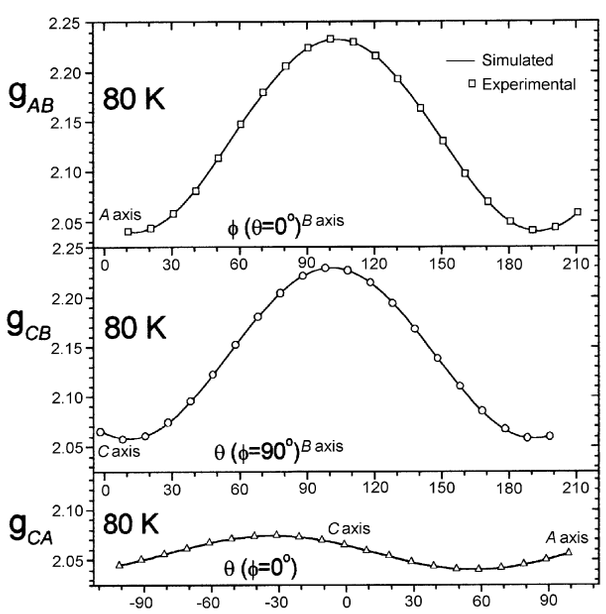

Fig. 7 Angular variation of the *g* values in the three orthogonal reference planes (*AB*, *CB*, *CA*) obtained from the EPR data for a $Cu_3(H_2L)(L)\cdot 2H_2O$ single crystal at 80 K. Continuous line are obtained by fitting the angular variation by the expression: $g^2 = g_{AA}^2\cos^2(\varphi) + g_{BB}^2\sin^2(\varphi) + 2g_{AB}^2\sin(\varphi)\cos(\varphi)$. The g^2 tensor is obtained from the parameters fitting in the three planes and diagonalized.

Conclusions

The fall in temperature until 100 K promotes subtle changes in the spacer arrangement of the tetra-deprotonated ligand unit in $Cu_3(H_2L)(L)\cdot 2H_2O$. Magnetic susceptibility studies indicate a strong antiferromagnetic interaction ($J/k = -194$ K) between the three copper ions in the bishelicate, as well as antiferromagnetic intermolecular interactions ($z'J'/k = -0.91$ K). Despite the existence of two magnetic types of copper(II) ions, only one signal is observed due to exchange effects. Below 100 K, the signal linewidth rapidly decreases and a typical exchange narrowed spectrum is observed at 4 K. The main contribution to the ground state wave function can be attributed to the $d_{x^2-y^2}$ orbitals, as expected for tetrahedrally distorted square planar Cu(II) chromophores.

Experimental

Crystal structure determinations

A single crystal of $[Cu_3(H_2L)(L)]\cdot 2H_2O$ was studied by X-ray diffraction techniques at 100 and 293 K on a Bruker P4 diffractometer equipped with a Smart CCD area detector. Crystal data, data collection and refinement parameters are summarized in Table 3. In both cases, the structure was solved by standard direct methods, followed by normal difference Fourier techniques,[21] revealing an asymmetric unit containing half a molecule, with the central Cu(2) lying on a two-fold axis. Full matrix, least-squares refinement was carried using anisotropic parameters on all non-H atoms. Hydrogen atoms on carbon atoms were included as fixed contributors in calculated positions using a riding model, except H-atoms bond to O-atoms, which were directly identified on Fourier maps, and their isotropic displacement parameters refined. Figures were drawn using ORTEP3 and RasWin.[22]

CCDC reference numbers 153196 and 153197.

See http://www.rsc.org/suppdata/dt/b1/b106983g/ for crystallographic data in CIF or other electronic format.

Physicochemical measurements

Magnetic susceptibility measurements were performed on pulverized crystalline samples in the range 2–300 K with a Quantum Design MPMS-5 SQUID magnetometer. The magnetic field used in the experiments was of 0.1 T, a value at which the magnetization *versus* magnetic field curve was still linear at 2 K. Experimental susceptibility values were corrected for the diamagnetic contributions and for the temperature-independent paramagnetism. The molar magnetization was also measured as a function of the magnetic field up to 5 T at 2 K.

Powder EPR spectra were obtained using a Varian E-109 spectrometer, equipped with a rectangular resonant cavity and 100 kHz field modulation and an ITC503 Oxford cryogenic system to vary the temperature. A HP5352B frequency counter was used to measure the microwave frequency. A powder sample of $Cu_3(H_2L)(L)\cdot 2H_2O$ was submitted to temperature variation from 4.4 K up to room temperature. The EPR spectra were acquired and digitized by a microcomputer equipped with a standard data acquisition card with an analogue-to-digital converter. The positions and linewidths of the resonances were calculated by numerical simulation of the spectra using the QPOW program.[23,24] A Bruker Elexsys E-580 spectrometer equipped with a cryogenic system and a goniometer were used to perform the single crystal EPR measurements at 9.4 GHz (X-band) with temperature and angular variations. A small single crystal (0.2 × 0.2 × 0.5 mm) was fixed with vacuum grease in a well cut KCl crystal to obtain a three orthogonal reference system (named *AB*, *CB*, *CA*) and was properly mounted in the goniometer.

Acknowledgements

Authors would like to thank the Xunta de Galicia (Spain) (XUGA 20903B99) and FAPESP and CNPq (Brazil) financial agencies.

Table 3 Crystal data and structure refinement for $[Cu(H_2L)(L)]\cdot 2H_2O$

T/K	100(2)	293(2)
Empirical formula	$C_{36}H_{38}Cu_3N_4O_{10}$	$C_{36}H_{38}Cu_3N_4O_{10}$
Formula weight	877.32	877.32
Wavelength/Å	0.71073	0.71073
Crystal system	Monoclinic	Monoclinic
Space group	$C2/c$	$C2/c$
a/Å	17.126(3)	17.171(3)
b/Å	13.809(3)	13.918(3)
c/Å	15.151(3)	15.373(3)
α/°	90	90
β/°	109.934(4)	110.026(5)
γ/°	90	90
V/Å^3	3368.4(11)	3451.6(12)
Z	4	4
D_c/Mg m^{-3}	1.730	1.688
μ(Mo-Kα)/mm^{-1}	1.945	1.898
θ Range/°	1.94–30.52	1.93–30.59
Reflections collected/unique	22 274/5122 (R_{int} = 0.0612)	22 891/5268 (R_{int} = 0.0754)
Data/restraints/parameters	5122/0/262	5268/0/272
Final R indices [$I > 2\sigma(I)$]	R_1 = 0.0361, wR_2 = 0.0877	R_1 = 0.0397, wR_2 = 0.0928
R indices (all data)	R_1 = 0.0623, wR_2 = 0.1002	R_1 = 0.1019, wR_2 = 0.1188

References

1 E. I. Solomon, *Dinuclear Copper Active Site in Copper Proteins*, T. G. Spiro, ed., Wiley-Interscience, New York, 1981, ch. 2.
2 F. L. Urbach, *Metal Ions in Biological Systems, No. 13. Copper Proteins*, H. Sigel, ed., Marcel Dekker, Basle, 1981.
3 K. D. Karlin and J. Zubieta, *Copper Coordination Chemistry and Biochemistry: Biochemical and Inorganic Perspectives*, Adenine Press, New York, 1983.
4 D. E. Fenton, *Advances in Inorganic and Bioinorganic Mechanisms*, A. G. Sykes, ed., Academic Press, London, 1983, vol. 2.
5 R. D. Willet, D. Gateschi and O. Khan, *Magneto-structural Correlations in Exchange Coupled Systems*, Nato ASI Series, Reidel, Dordrecht, 1983.
6 K. D. Karlin and J. Zubieta, *Biological and Inorganic Copper Chemistry*, Adenine Press, New York, 1986, vols. 1 and 2.
7 P. A. Vigato, S. Tamburini and D. E. Fenton, *Coord. Chem. Rev.*, 1990, **106**, 25.
8 C. E. Niederhoffer, J. H. Timmons and A. G. Martell, *Chem. Rev.*, 1984, **84**, 137.
9 R. Malkin and B. G. Malmström, *Adv. Enzymol.*, 1990, **33**, 177; B. Reinhammar, *Copper Proteins and Copper Enzymes*, CRC Press, Boca Raton, FL, 1982, vol. 3, pp. 1–35; A. Messerschmidt, A. Rossi, R. Ladenstein, R. Huber, M. Bolognesi, G. Gatti, A. Marchesini, R. Petruzelli and A. Finazzo-Agró, *J. Mol. Biol.*, 1989, **206**, 513; A. Messerschmidt, R. Ladenstein, R. Huber, M. Bolognesi, G. Gatti, A. Rossi and A. Finazzo-Agro, *J. Mol. Biol.*, 1992, **224**, 179.
10 I. Gromov, A. Marchesini, O. Farver, I. Pecht and D. Goldfarb, *Eur. J. Biochem.*, 1999, **266**, 820; J. L. Cole, P. A. Clark and E. I. Solomon, *J. Am. Chem. Soc.*, 1990, **112**, 9534; J. L. Cole, L. Avigliano, L. Morpurgo and E. I. Solomon, *J. Am. Chem. Soc.*, 1991, **113**, 9080.
11 P. V. Bernhardt and P. C. Sharpe, *J. Chem. Soc., Dalton Trans.*, 1998, 1087.
12 J. Sanmartín, M. R. Bermejo, A. M. García-Deibe, O. Piro and E. E. Castellano, *Chem. Commun.*, 1999, 1953.
13 U. Casellato, P. Guerriero, S. Tamburini, S. Sitran and P. A. Vigato, *J. Chem. Soc., Dalton Trans.*, 1991, 2145.
14 P. Guerriero, S. Tamburini, P. A. Vigato, U. Russo and C. Benelli, *Inorg. Chim. Acta*, 1993, **213**, 279.
15 J. Sanmartín, M. R. Bermejo, A. M. García-Deibe, M. Maneiro, C. Lage and A. J. Costa-Filho, *Polyhedron*, 2000, **19**, 185.
16 K. Ueno and A. E. Martell, *J. Phys. Chem.*, 1955, **59**, 998; K. Ueno and A. E. Martell, *J. Phys. Chem.*, 1956, **60**, 1270; D. X. West and M. D. Owens, *Transition Met. Chem.*, 1998, **23**, 87.
17 K. Bertoncello, G. D. Fallon, K. S. Murray and E. R. T. Tiekink, *Inorg. Chem.*, 1991, **30**, 3562; W. Mazurek, K. J. Berry, K. S. Murray, M. J. O'Connor, M. R. Snow and A. G. Wedd, *Inorg. Chem.*, 1982, **21**, 3071.
18 L. S. Long, S. P. Yang, Y. X. Tong, Z. W. Mao, X. M. Chen and L. N. Ji, *J. Chem. Soc., Dalton Trans.*, 1999, 1999.
19 K. Kambe, *J. Phys. Soc. Jpn.*, 1950, **5**, 48.
20 R. L. Carlin, *Magnetochemistry*, Springer, Berlin, 1986.
21 G. M. Sheldrick, SHELX97 Programs for Crystal Structure Analysis, University of Göttingen, Germany, 1997.
22 L. J. Farrugia, *J. Appl. Crystallogr.*, 1997, **30**, 565; R. Sayle, RasWin Molecular Graphics, Windows Version 2.6-ucb, 1993.
23 M. J. Nilges, PhD Thesis, University of Illinois, Urbana, IL, 1979.
24 R. L. Belford and M. J. Nilges, *Computer Simulation of Powder Spectra*, EPR Symposium, 21st Rocky Mountain Conference, Denver, CO, August 1979.